ACS OMEGA

Open Access

http://pubs.acs.org/journal/acsodf

Article

Fine-Tuning Filter Cake Sealing Performance: The Role of Particle Size in Hematite Weighted Water-Based Drilling Fluid

Jaber Al Jaberi, Badr Bageri,* Waleed Otain, Anas Alsaleem, and Abdulrauf Rasheed Adebayo

Cite This: *ACS Omega* 2024, 9, 25084−25093

Read Online

ACCESS | Metrics & More | Article Recommendations

ABSTRACT: Three hematite grades with different particle sizes (i.e., large, medium, and small) were evaluated, and the selection criterion was median particle size. The investigation involves the following stages: rheology, filtration, and filter cake formation. Different rheological models including Bingham, Power law, Herschel−Bulkley, and Robertson−Stiff were implemented to find the optimum model for characterizing fluid behavior. The results showed that medium-sized hematite particles produced the highest filtration volume, filter cake thickness, and filter cake permeability. These results were confirmed when a varied pore distribution filtration medium was used. The NMR results showed the same trend where the highest reduction in core porosity was found when a medium-size particle distribution was used. There is a minimum alteration in the rheological behavior of the drilling fluid as the particle size was varied, and the drilling fluids showed a shear-thinning behavior and were best described by the Herschel−Bulkley model. Particle size ratio emerges as a key factor for controlling and enhancing the filtration properties and filter cake characteristics.

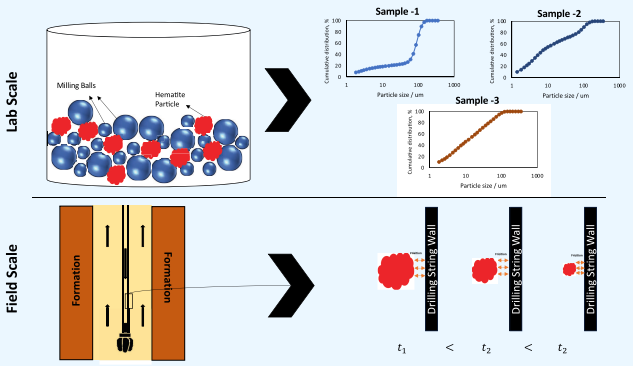

1. INTRODUCTION

Hematite is one of the common earth iron minerals (α-Fe_2O_3) that is found abundantly in several places around the globe, particularly in high-grade hematite iron deposits located in Brazil, South Africa, and India. The formation process of this mineral is explained by various theories, such as diagenetic, deep-seated hydrothermal, and supergene processes.[1−3] Hematite possesses many distinctive features, including high stability, environmental friendliness, preferential bandgap structures, high theoretical capacities, and cost-effectiveness. Due to its unique characteristics, hematite has become a promising addition to numerous applications including carbon capture/storage, solar photoelectrochemical (PEC) cells, photoelectrochemical water splitting, and photocatalytic, among others.[4−10] With its high specific weight, hematite also serves as an excellent weighting material for drilling and cementing operations in the oil and gas industry.[11]

Scharf and Watts (1984) were among the first to report the usage of hematite (also called Itabirite) as a weighting material for oil-based mud.[12] They used it to formulate high-density mud (i.e., 18 ppg) and compared its performance with Barite drilling fluid. The results showed that hematite had lower rheology and electrical stability compared with Barite mud. The higher abrasiveness of hematite compared with Barite was a shortcoming, but the hematite improved the penetration rate that reflected positively on the economic aspect of drilling operation. Tovar et al. tested hematite natural deposits in Venezuela, and all the tests' results confirmed the previous conclusion on both laboratory and field scales with an additional benefit of hematite causing less formation damage and lower environmental impact. The abrasiveness was higher than Barite but did not have a huge impact on the conducted field trials.[13] Fadl et al. used delaminated iron ore (hematite-Barite) as a weighting material and investigated its performance on density, fluid loss, filter cake, stability, and rheological properties.[14] The delaminated iron ore consists mainly of Fe_2O_3 and BaO (i.e., 69.76 and 14.17%, respectively), and it has a specific gravity equal to 4.67. They tested the delaminated iron ore at an extensive range of density (9.6−18.7 ppg) and temperature (ambient to 180 °F). The results demonstrated the potential of iron ore as a weighting material, as it gave an acceptable result in comparison to Barite mud with respect to filtration loss, filter cake thickness, and stability. However, the yield point and gel strength showed higher values, which might negatively affect the operations, but this

Received: March 11, 2024
Revised: May 19, 2024
Accepted: May 22, 2024
Published: May 30, 2024

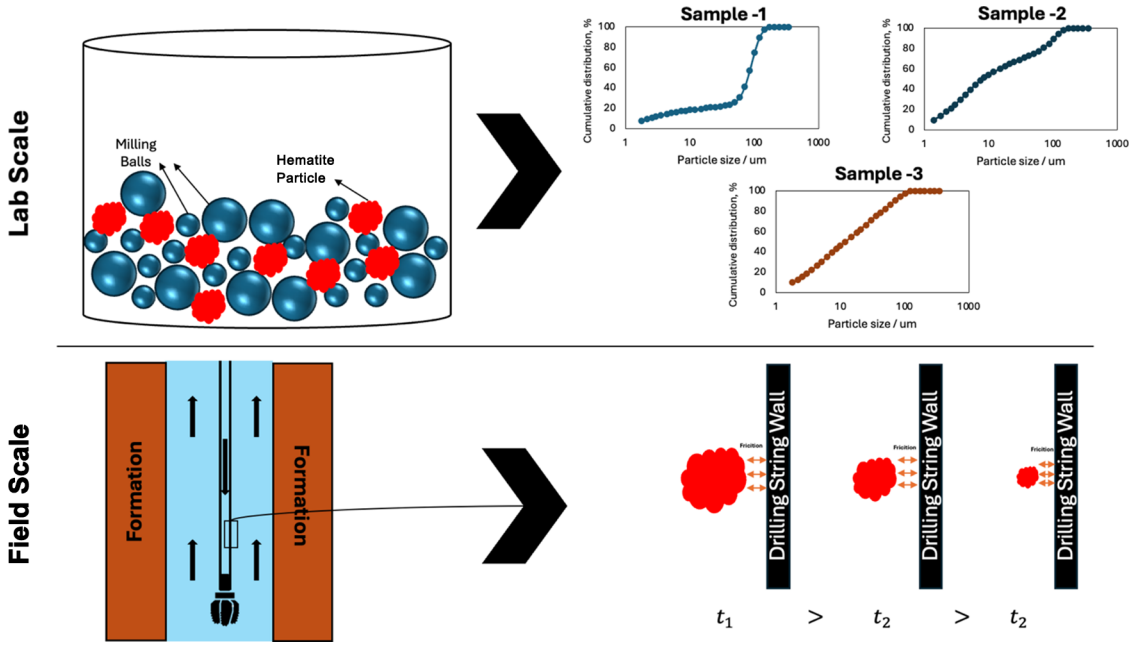

Figure 1. Mechanism of changing the particle size on the laboratory and field scales.

depends on the density and can be remedied by use of an additive or by mixing with Barite as a weighting material.

The abrasiveness of hematite can cause gradual erosion to different parts of the surface equipment. Quercia et al. investigated four different particle size distributions (PSD) of hematite samples and contrasted the result with commercial Barite samples.[15] They used the statistical parameter D_{90} as the base for the comparison, and they used these samples to form an oil-based drilling fluid with a density of 1977.1 kg/m^3 (i.e., ∼16.5 ppg). They tested these samples in erosion tests using a test loop at different angles, and the assessment of the wear was performed using weight loss and laser profilometry. The results showed that there is an ability to minimize erosion rate by controlling the particle size distribution of hematite. Particle sizes at D_{90} (38 μm) resulted in an erosion equal to the Barite erosion profile, while a field trial was successful when a D_{90} value of 30 μm was utilized. Tehrani et al. performed an extensive study comparing the performance of ilmenite and hematite with API Barite grade.[16] They formulate two based muds (i.e., water and oil-based) using these weighting materials, and they investigate relative abrasiveness, magnetic feature, and the various size grades impact on the rheology, fluid loss, and stability of the mud. Their results showed that hematite and ilmenite can give excellent performance that is close to and sometimes even better than Barite when it comes to rheology and fluid loss at the right range of PSD. Both ilmenite and hematite exhibited a higher tendency to sag under static and dynamic conditions with high abrasiveness, the recommended size to minimize these issues and have good drilling properties is D_{95} of 25 μm. The PSD of the solids may change during the mud circulation process (degradation) due to friction with various tools, and this may induce a loss of circulation and formation damage. Kang et al. examined the factors that impact the degradation of calcium carbonate particles. They used the changes in D_{90} as the evaluation criterion.[17] They found that the highest impact factors are rotation speed, shear time, and initial particle size, while other factors such as salinity, temperature, pH, and concentration have minimum effects. Furthermore, they established a critical particle size (i.e., D_{90} equals 15−20 μm), beyond which there is no further degradation. Consequently, it is imperative to conduct a more systematic analysis of how particle size impacts drilling fluid performance. This entails examining a broader range of Particle Size Distributions (PSDs) and understanding their effects on the properties of drilling fluids.

In this study, we explored a broad spectrum of hematite particle size distributions to determine their effect on drilling fluid performance. A variety of tests and equipment were employed to characterize the different hematite particles and assess their performance. Furthermore, two types of filtration media were used to investigate how these hematite particle sizes functioned within different porous media.

2. METHODOLOGY

This section describes the methodology implemented in this study, which is divided into two key areas: preparation of the drilling fluid and evaluation of its properties. The first part addresses the selection and characterization of materials including hematite and drilling fluid formulations. The second part details the equipment and experimental procedures used to assess the properties of the drilling fluid.

2.1. Drilling Fluid Preparation. *2.1.1. Preparation and Characterization of Hematite Samples.* Since the focus of this work is mainly on the particle size distribution, great effort was made in the preparation and characterization of the hematite particles. This involved several stages to ensure that they have various particle grades. Initially, the hematite raw sample was collected and examined using scanning electron microscopy (SEM), X-ray fluorescence (XRF) analysis, X-ray diffraction (XRD) analysis, densitometer, and particle size analyzer to determine the shape, material composition, mineral composition, density, and particle size distribution, respectively. The SEM results showed that the hematite particle has an irregular shape and consists mainly of iron (Fe), which represents 96%, and the remaining 4% are traces of aluminum and silicon. The XRD confirmed that the sample mineralogy is

https://doi.org/10.1021/acsomega.4c02352
ACS Omega 2024, 9, 25084−25093

100% hematite, and the densitometer result showed a specific gravity equal to ∼4.9 for hematite particles. The PSD analyzer showed the raw hematite had a wide range, the three main percentiles of particle D_{10}, D_{50}, and D_{90} are equal to 12, 212, and 542 μm, respectively. Hence, to obtain acceptable hematite grades, an iterative series of experiments were performed that included ball milling and sieve analysis to change the size and then PSD analysis and SEM to evaluate the sizes.

Hematite particles are known to have high hardness in comparison to Barite. It has a value of 5−6 on the Mohr scale and almost 886 on the Vickers hardness scale.[15] The ball milling process confirmed this, as it was quite strenuous to change the PSD of hematite particles. This can be considered an advantage since it limits the degradation of the hematite particles. Many machine runs were performed to change the particle size, and several of them failed to change the PSD. From another angle, this indicates that the degradation of the hematite particles during the circulation of the mud is less likely. It depends on many factors including the rheological properties, density (i.e., solid concentration), and the flow regime.[15,18] The degradation phenomenon occurs during the circulation process, which is mimicked in the laboratory by the ball milling machine process as shown in Figure 1.

The middle percentile (i.e., D_{50}) was used to determine the grades in this work. Initially, the hematite sample was milled for 30 min, and then, a sieve analysis was performed for different sizes. Afterward, different samples were collected and a PSD analyzer was utilized to assess the new distribution. If the target distribution was not achieved, then the process was repeated. Whenever a new particle size was obtained, SEM was employed to ensure that there was no significant change in the particle shape to have a fair comparison between them. This process is summarized in Figure 2. After many trials, a new

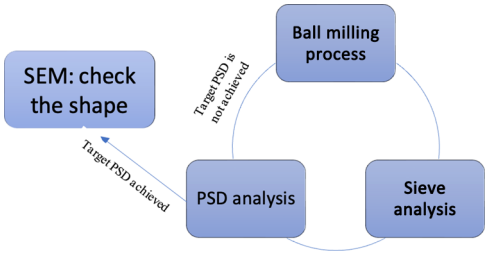

Figure 2. Method to obtain different hematite grades.

particle grade was obtained that was labeled as large, with D_{10}, D_{50}, and D_{90} corresponding to 2.4, 79.8, and 123.5 μm, respectively. The second grade was labeled as a medium with D_{10}, D_{50}, and D_{90} equal to 1.8, 12.0, and 70.8 μm, respectively. The final grade was labeled as small in which D_{10}, D_{50}, and D_{90} were equal to 1.4, 8.0, and 103.4 μm, respectively. All the three grades' distributions are shown in Figure 3. The SEM results showed that there were no significant changes to the particle's shape as shown in Figure 4.

2.1.2. Drilling Fluid Preparation. Drilling fluid formulations were then prepared using the previously generated three grades of hematite particles. Starting with the aqueous phase, 331.4 mL of water was used, and 0.1 mL of defoamer was added to prevent foam formation. Soda ash and potassium hydroxide were added to the formulation for pH control, while xanthan gum (XC) and bentonite function were used to control the rheology. Starch and PAC-R roles were added to improve the filtration and filter cake properties. Potassium chloride serves to minimize clay swelling, while calcium carbonate works as a bridging material. Finally, the obtained different grades of hematite (i.e., large, medium, and small) were used as a weighting material to increase the mud density. Drilling fluid formulations that contained hematite of large, medium, and small grades are labeled as mud-1, mud-2, and mud-3, respectively. Table 1 shows the order and quantity of each drilling fluid component. Note that the three formulations have the same mud components, with the difference being only the hematite particle grades.

2.2. Drilling Fluid Properties. The properties of the mud that were investigated are the rheological and filtration properties. The Grace viscometer was used to obtain the various rheological parameters, which gives the dial readings at different speeds and the gel strength at different times (i.e., 10 s, 10 min). The dial reading at different speeds was used to obtain the plastic viscosity and yield point using the following formula:

$$\mathrm{PV} = \text{Ø}_{600} - \text{Ø}_{300} \tag{1}$$

$$\mathrm{YP} = \text{Ø}_{300} - \mathrm{PV} \tag{2}$$

The test was conducted at a temperature of 120 °F and a pressure of 14.7 psi.

For the filtration test, an HTHP (high-temperature, high-pressure) filter press was used to run the fluid loss test for two different filtration media (i.e., a ceramic disk and a rock core sample). The procedure is the same for both filtration media. The mud sample was placed inside the cell and pressurized to the desired pressure using nitrogen gas. A heating jacket placed around the cell heated the cell until the required temperature was reached; then, the outlet valve was opened where the mud filtrate passed through the filtration medium and collected at the other end of the filtration media. Each filtration test lasted for 30 min, and a filter cake was built up on the upstream end of the ceramic disk or rock core sample. The filter cake was then taken out, and the filtration volume was collected and plotted against time. The produced filter cake was then examined to measure its thickness, while its permeability was calculated using the following equation:[19]

$$K_{\mathrm{fc}} = 14{,}700\frac{q^{*}\mathrm{Th}_{\mathrm{fc}}{}^{*}\mu}{p_{\mathrm{fc}}} \tag{3}$$

where K_{fc}, $\mathrm{Th}_{\mathrm{fc}}$, μ, q, and p_{fc} are the permeability (mD) and thickness (cm), filtrate viscosity (cP), filtration rate per area unit (cm/s), and differential pressure (psi), respectively.

The conditions of the tests are a differential pressure of 300 psi and a temperature of 250 °F. The properties of the two filtration media are listed in Table 2.

3. RESULTS AND DISCUSSION

In the first subsection, we delve into the filtration aspects using both the ceramic disk and the Berea core sample as filtration media for each mud sample. The following subsection focuses on the rheological aspects, encompassing key properties, such as plastic viscosity, yield point, and gel strength. Furthermore, various rheological models were employed to enhance our understanding of the mud's rheological behavior as a function of PSD.

3.1. Filtration Properties. It is worth noting again that the different drilling muds have similarities in their components, as

https://doi.org/10.1021/acsomega.4c02352
ACS Omega 2024, 9, 25084−25093

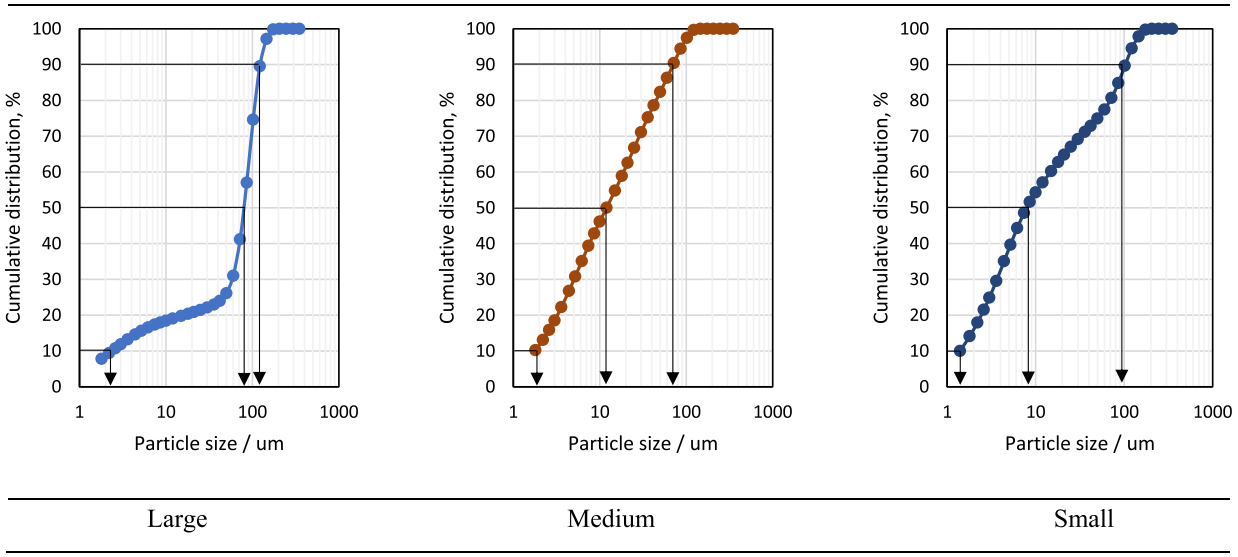

Figure 3. Particle size distribution of hematite grades.

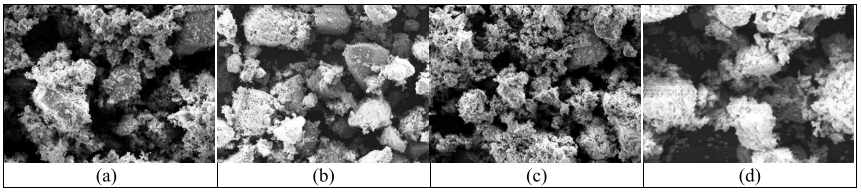

Figure 4. SEM image for the three hematite grades (a: raw, b: large, c: medium, d: small).

Table 1. Drilling Fluid Composition Was Used to Prepare One Barrel

component	amount		
mud ID	mud-1	mud-2	mud-3
water, mL	331.4		
defoamers, mL	0.1		
soda ash, gm	0.5		
XC, gm	0.5		
starch, gm	6		
bentonite, gm	4		
KOH, gm	0.5		
PAC-R, gm	1		
KCl, gm	20		
$CaCO_3$ (25 μm) gm	2.5		
$CaCO_3$ (50 μm) gm	2.5		
hematite, gm	95.3		
	large particles	medium particles	small particles

shown in Table 1, except for the different particle sizes. In the first phase, the filtration tests were conducted utilizing a ceramic disk with a uniform pore distribution to isolate the effect of varying pore size of the filtration medium. Hence, the role of only the particle size can be examined. In another test, a reservoir rock core sample with a distribution of pore sizes was employed to replace the ceramic disk. A natural rock core sample introduces variability in pore and throat sizes adding a layer of complexity and providing a more realistic representation of the conducted tests. Moreover, the ability to control the length of core samples facilitates the usage of advanced techniques such as nuclear magnetic resonance (NMR) to evaluate the properties of the rock after intrusion by the mud filtrates.

The filtration performance of the three mud formulations is depicted in Figure 5 for both filtration media (ceramic disk and rock core). The total filtration volumes for mud-1, mud-2, and mud-3 were 8.7, 9.2, and 8.6 mL, respectively. Notably, mud-2 (i.e., with medium hematite particle size) exhibited a slightly higher value among the other two mud formulations, which was potentially attributed to its hematite particle size distribution. Similarly, the use of rock core samples as the filtration medium showed more distinct filtration behavior. Mud-2 produced the highest filtration volume (13.8 mL) compared with mud-1 and mud-3, both of which produced 4.8 mL of filtrates.

Figures 6 and 7 illustrate the thickness and calculated permeability of the filter cake for both filtration media. The

Table 2. Properties of Filtration Media

	ceramic disk		core sample		
muds	pore throat, μm	permeability, D	type	porosity, %	permeability, mD
mud-1	20	3	Berea sandstone	20.5	156.4
mud-2				22.1	130.8
mud-3				20.6	153.1

https://doi.org/10.1021/acsomega.4c02352
ACS Omega 2024, 9, 25084−25093

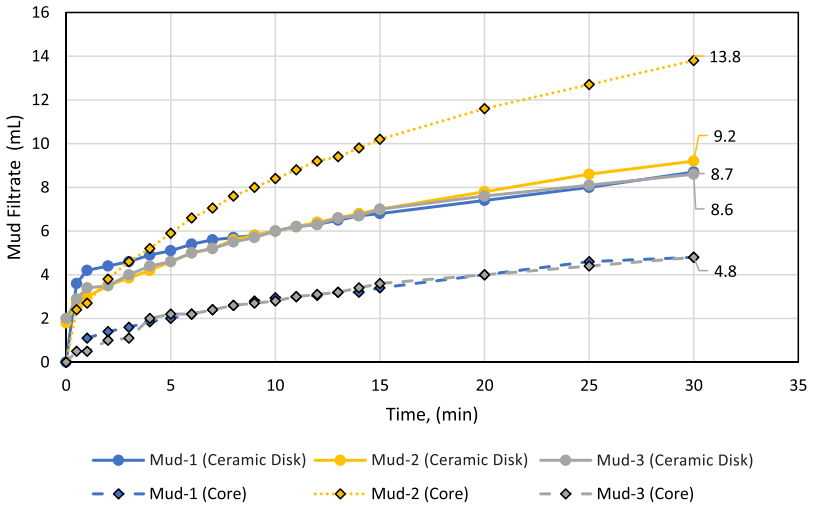

Figure 5. Filtration behavior.

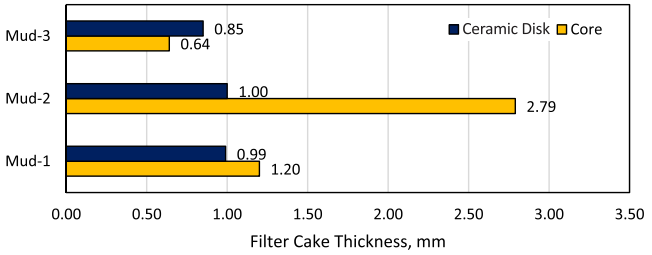

Figure 6. Filter cake thickness for the investigated base drilling fluids.

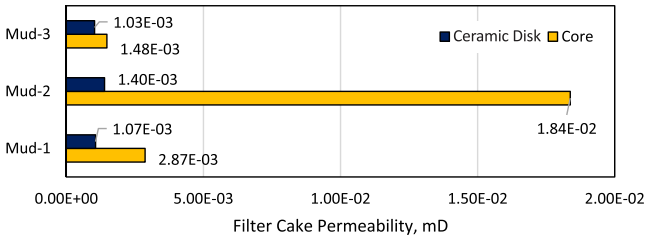

Figure 7. Filter cake permeability for both filtration media.

filter cake thickness with the ceramic disk is very close for the three muds falling in the range of 0.85−1 mm. On the other hand, the thicknesses of the filter cake formed on core samples showed wider variation, in which mud-2 formed the thickest filter cake (2.79 mm) compared with mud-1 and mud-3, 1.2 and 0.64 mm thickness, respectively. Similarly, the estimated filter cake permeability showed the same trends for both filtration mediums. Mud-2 exhibited the highest permeability values (1.84 and 0.14 mD for core and ceramic disk, respectively), while mud-3 displayed the lowest permeability values of filter cake among the other formulations (0.00103 and 0.00148 mD for core and ceramic disk, respectively). The remaining formulation (i.e., mud-1) had the intermediate filter cake permeability values, with the value of 0.00287 mD for the core and 0.00107 mD for the ceramic disk.

In addition to providing a more realistic filtration medium (similar to downhole reservoir conditions), using a reservoir core sample as a filtration medium allows the application of benchtop NMR to probe the effects of filtration into the pores of the porous medium. A core sample with a sufficient length provides the sample volume needed for a good signal-to-noise ratio during NMR measurements. Following the method outlined by Adebayo and Bageri[20] and Adebayo et al.,[21,22] the NMR T_2 distribution measured at different stages of the experiment provides valuable insight into the filter cake porosity and the degree of invasion. In summary, the core sample passes through three stages of NMR scanning namely: (i) pretest with 100% brine saturation sample, (ii) mud filtrate

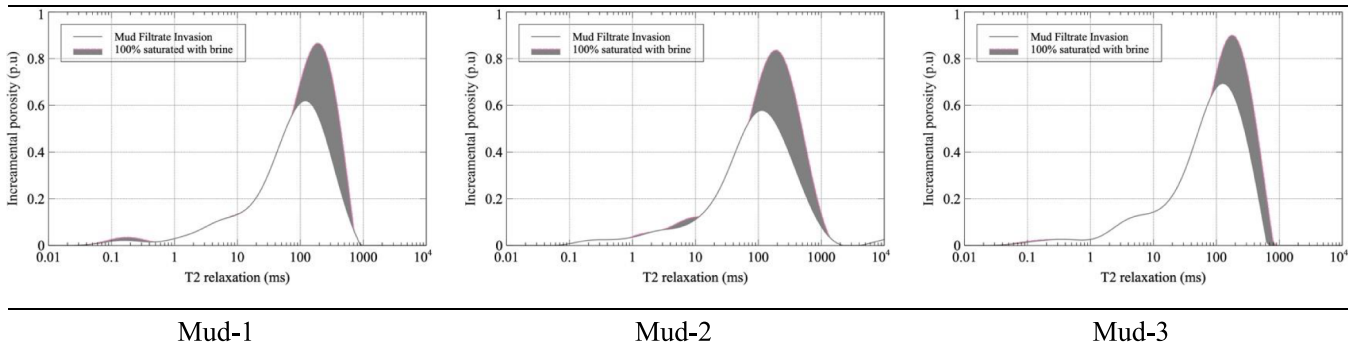

Figure 8. NMR T_2 curve at the initial stage (when the sample is 100% saturated with water) overlain by the T_2 curve at the last stage (when the sample has been infiltrated with filtrates and particles from the mud). The gray area represents the difference between the two curves, which characterizes the T_2 (corresponding to the pore size) distribution of the pores damaged by solid invasion.

https://doi.org/10.1021/acsomega.4c02352
ACS Omega 2024, 9, 25084−25093

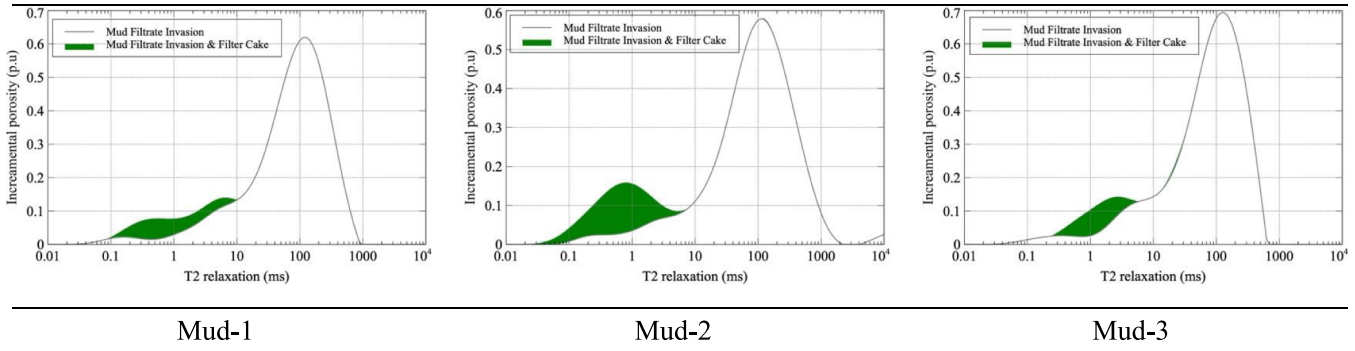

Figure 9. NMR T_2 curve of the rock sample after mud filtrate invasion and with the deposited filter cake overlaid by the T_2 curve of the sample after the filter cake was removed. The green area represents the difference between the two curves that characterize the T_2 (corresponding to the pore size) distribution of the filter cake.

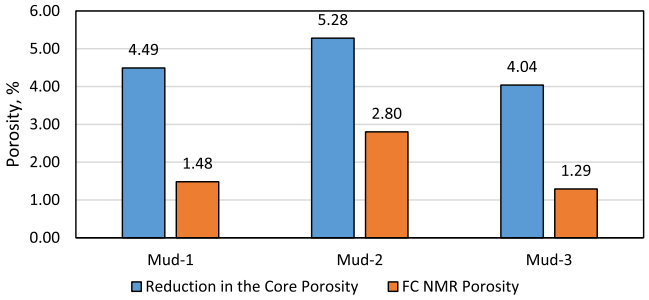

Figure 10. Porosity values for the core and filter cake are estimated by NMR for each drilling formulation.

invasion into the pores plus filter cake deposited at the upstream end of the core, and (iii) core sample only after removing the filter cake. Figures 8 and 9 present the NMR T_2 profiles of the rock core sample at different NMR scanning stages for each drilling formulation. The shaded areas in the curve represent the differences (by subtraction) between the two T_2 curves shown in each figure. The difference in the T_2 curve of a 100% water-saturated sample and the T_2 curve of the same sample after mud infiltration shows the pores damaged by particle invasion (gray area in Figure 8). Similarly, the difference between the T_2 curve of the same sample after mud infiltration (but with the filter cake on top) and the T_2 curve after the filter cake was removed represents the T_2 distribution (equivalent to pore size distribution) of the filter cake (green area in Figure 9). Mud-3 invaded a single-pore system (corresponding to T_2 > 80 ms), resulting in the lowest porosity reduction (4.04%) due to the invasion of only the big pores. However, the invasion by mud-1 and mud-2 occurred in two pore systems (mud-1:0.1 ms < T_2 < 1 ms and T_2 > 50 ms; mud-2:1 ms < T_2 < 10 ms and T_2 > 70 ms). Thus, mud-1 and mud-2 caused the highest porosity reduction corresponding to 4.49 and 5.28% respectively. Furthermore, mud-3 generated a filter cake with the lowest porosity (i.e., 1.29%), while mud-2 had the highest filter cake porosity (2.8%). Mud-1 filter cake porosity lies (2.8%) with an invasion-induced porosity reduction of 5.28%. The previous results showed mud-2 has different behavior in terms of filtration volume and filter cake

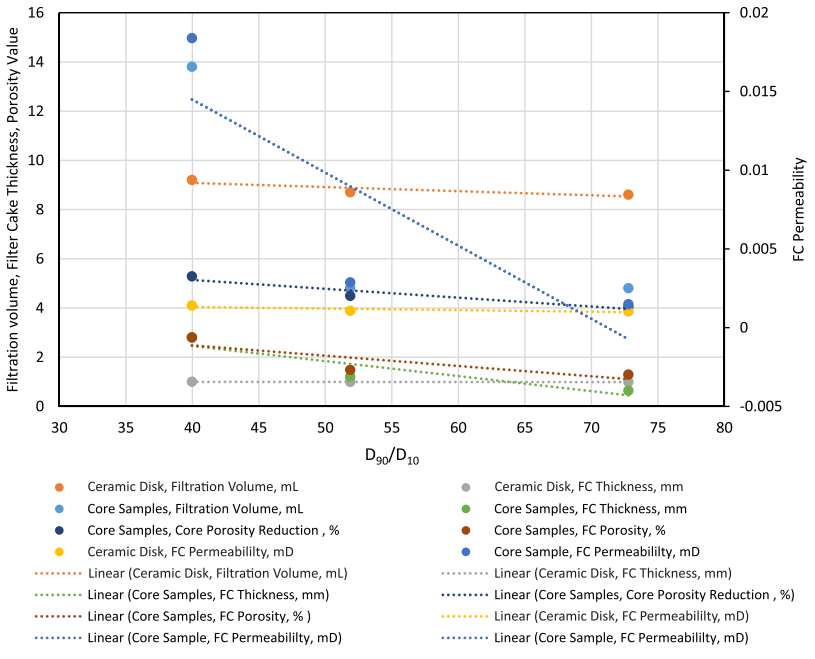

Figure 11. Filtration volume, filter cake thickness, filter cake porosities, and permeabilities vs the ratio of particle size at different percentiles.

https://doi.org/10.1021/acsomega.4c02352
ACS Omega 2024, 9, 25084−25093

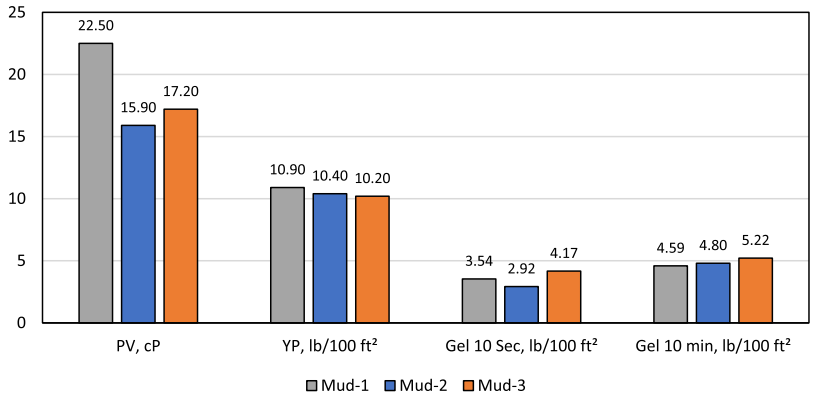

Figure 12. Rheological properties for the drilling fluid formulations.

Table 3. Rheological Models[a]

#	model	relation	constrain
1	Bingham	$\tau = \tau_0 + \mu_\infty \gamma$	$\tau_0 \geq 0$ $\mu_\infty > 0$
2	Power law	$\tau = K\gamma^n$	$K > 1$ $0 < n < 1$
3	Herschel–Bulkley	$\tau = \tau_0 + K\gamma^n$	$\tau_0 \geq 0$ $K > 0$ $0 < n < 1$
4	Robertson-Stiff	$\tau = A(\gamma + C)^B$ $(\tau > AC^B)$ $\gamma = 0$ $(\tau \leq AC^B)$	$A > 0, 0 < B < 1, C \geq 0$

[a] τ: shear rate. γ: shear stress. K: consistency index. n: flow behavior index. μ_∞: plastic viscosity. τ_0: excess shear stress. A, B, C: numerical parameters.

features for core samples compared with other mud formulations; the justification of such behavior comes down to the hematite particle range, pore throat, and pore distribution. The medium hematite particle grade range is narrower than the large and small grades, the difference between D_{90} and D_{10} is 68.1 μm compared with 122.7 and 101.9 μm for large and small, respectively. The wider range of particles made it easier to have more compacted filter cake since the different particles can fill the pores, which can be seen in the low filter cake porosity for mud-1 and mud-3. Pore throat was not measured in this work, yet it can be estimated using the Winland equation that depends on core porosity and permeability.[23] The core pore throat used for mud-1, mud-2, and mud-3 is 13.7, 12.7, and 13.7 μm. Associating each core pore throat with used particle distribution showed the difference in the case of mud-2. Klungtvedt and Saasen showed the importance of the D_{90}/pore size ratio that can impact the filtration results, using a similar argument (i.e., D_{90}/pore size or D_{90}/D_{10}/pore size), and showed the ratio is the lowest for mud-2 compared with other formulations.[24] Finally, the core pore distribution used for mud-2 showed that pore system, transfer relaxation time measurement (T_2) exceeded 900 ms in comparison to other used cores, and T_2 have a direct relation to the rock pore size.[25]

These porosity numbers are summarized in Figure 10. It is worth mentioning that these values of rock porosity (after hematite invasion and filter cake deposits) are likely affected by the enhanced relaxation caused by the hematite. Hematite is a paramagnetic material and thus affects the NMR signal by causing an internal magnetic gradient in the rock, which eventually causes faster relaxation.[26] Hence, the reported decrease in porosity may be overestimated. Nonetheless, since the intention here is to compare three mud systems (all having hematite), the comparison is valid in that we can see how each of the mud formulations affects the filter cake and particle invasion. The use of low-field NMR (2 MHz) in this study also dampens, to some extent, the effect of the paramagnets on the measured NMR relaxation.

Numerous factors contribute to the previously investigated properties, encompassing filtration medium permeability and porosity, pore size distribution, and particle size distribution, among others. Among these factors, the particle size

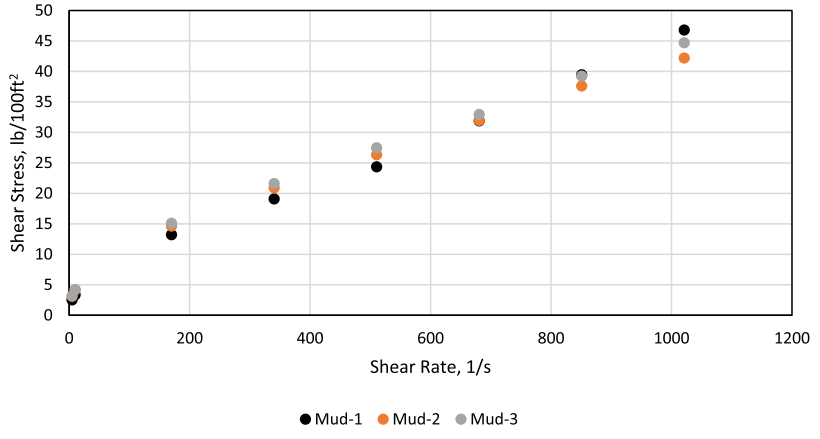

Figure 13. Shear stress vs shear rate for three drilling formulations.

https://doi.org/10.1021/acsomega.4c02352
ACS Omega 2024, 9, 25084−25093

Table 4. Bingham Plastic, Power Law, Herschel–Bulkley, and Robertson-Stiff Models Rheological Model's Parameters and Their Evaluation Criteria for Each Drilling Formulations

		Bingham plastic			Power law				Herschel–Bulkley					Robertson-Stiff			
mud type	PV	YS	RMSE	R^2	K	n	RMSE	R^2	K	n	YS	RMSE	R^2	A	B	C	RMSE	R^2
mud-1	0.04	3.65	1.30	0.994	0.21	0.78	1.79	0.990	0.08	0.91	2.82	1.24	0.996	0.09	0.89	49.37	1.28	0.996
mud-2	0.04	5.65	2.21	0.980	0.67	0.59	1.08	0.995	0.33	0.69	2.43	0.50	0.999	0.46	0.65	17.53	0.58	0.999
mud-3	0.04	5.61	2.18	0.983	0.62	0.61	1.21	0.995	0.30	0.71	2.53	0.65	0.999	0.42	0.67	18.99	0.73	0.998

distribution of hematite emerges as the controlling parameter, prompting an investigation of the potential relationships with other properties for improved outcomes. To establish correlations, different ratios of the particle size percentiles (i.e., D_{90}/D_{50}, D_{90}/D_{10}, and D_{50}/D_{10}) were investigated. The most meaningful relationships were identified when D_{90}/D_{10} was correlated to filter cake properties. Figure 11 illustrates these relationships, showcasing the correlations between the D_{90}/D_{10} ratio and filter cake thickness, reduction in core porosity (i.e., formation damage), filter cake NMR porosity, filtration rate, and filter cake permeability. Observing each property and how it correlates with this ratio reveal intriguing behavior. In general, each mud filtration property tends to decrease as the ratio increases, with certain properties displaying higher sensitivities to this change. Reduction in the core porosity and filter cake permeability emerges as the most sensitive to the ratio. These two properties are interconnected, as a higher filter cake permeability increases the possibility of drilling fluid invading the formation, resulting in a greater reduction in core porosity.

3.2. Rheological Properties. The rheological properties of the drilling fluids play a crucial role in various drilling functionalities, making it imperative to assess how changes in the PSD of the weighting material might affect these properties. Figure 12 shows an overview of key rheological properties for the investigated drilling formulations, including the plastic viscosity (PV), yield point (YP), PV/YP ratio, and gel strength at 10 s and 10 min. Minimal changes were observed in most rheological properties with varying particles' PSD. The most significant change was in PV values, where mud-1 exhibited the highest value (22.5 cP) compared with mud-2 and mud-3 (15.9 and 17.2 cP). YP values experienced a slight reduction as particle sizes decreased, moving from 10.9 lb/100 ft^2 for mud-1 to 10.4 and 10.2 lb/100 ft^2 for mud-2 and mud-3, respectively. Gel strength progression from 10 s to 10 min was acceptable for the formulations, increasing from 3.54, 2.93, and 4.17 to 4.59, 4.8, and 5.22 lb/100 ft^2 for mud-1, mud-2, and mud-3, respectively. Even though the previous results do not highlight the impact of the PSD on the rheology, the main reason might be attributed to the mud's low density (i.e., low solid packing and friction between the particles).

Beyond these basic rheological properties, various rheological models were employed to understand the drilling behavior and pressure losses during the drilling process. Several models are available in the literature, and each model has its advantages and disadvantages. Common models, such as the Power law model, Bingham model, Herschel–Bulkley model, and Roberston–Stiff model were utilized.[27−30] Table 3 shows the relations and constraints for the previously mentioned models. The shear rate and shear stress values of each mud formulation were fitted to these models using regression analysis (i.e., nonlinear least squares), with evaluation criteria including root-mean-square error (RMSE) and the coefficient of determination (R^2) to assess the performance of the investigated models.

Figure 13 depicts the shear stress versus shear rate for each drilling formulation, along with fitted models. Table 4 provides the rheological models' parameters and their evaluation criteria for each drilling formulation. The Bingham model considered the closest model to the Newton model compared with other models (i.e., straight line with intercept point), demonstrated excellent fit for all formulations in which the PV value was the same for all the drilling formulations, while YS values were

https://doi.org/10.1021/acsomega.4c02352
ACS Omega 2024, 9, 25084−25093

close for the three formulations. Since most of the models showed an acceptable performance, the limitations represented by the highest RMSE and lowest R^2 are discussed. The evaluation criteria were excellent for all the models and among all of the formulations with the highest RMSE and lowest R^2 equal to 2.21 and 0.994, respectively. These criteria improve more as well for the other models due to the improvement in the fitting capability. Power law had the highest RMSE equal to 1.79 and the lowest R^2 equal to 0.99 for mud-1. The model parameters (K) and (n) varied between the formulations, K was equal to 0.21, 0.67, and 0.62 for mud-1, mud-2, and mud-3, respectively, while the n was equal to 0.78, 0.59, and 0.61 for the same formulations order. The three models (i.e., Herschel−Bulkley model, Roberston-Stiff) had the highest accuracy represented by the lowest RMSE and the highest R^2. Since the Herschel−Bulkley model was the best in describing the fluid, it will be used to describe the parameter's performance. The K value represented the dependency of the shear stress on the shear rate, mud-1 has the lowest dependency compared with the other two drilling formulations. The cutting suspension ability of the mud is represented by the YP (experimentally) and YS (modeling) which is important in terms of cutting suspension and well stability. All formulations showed shear-thinning behavior since $n < 1$.

4. CONCLUSIONS

The role of hematite's PSD in drilling fluid performance is multifaceted, impacting various properties either positively or negatively. This detailed study delved into the nuanced effects of hematite PSD on drilling fluid filtration and rheological behavior through a comprehensive series of experiments. The findings underscore the pivotal role of PSD in influencing these properties. Particularly, the study revealed that the degradation of hematite particles halts at a D_{50} value of 8 μm, showcasing the unique characteristics of hematite in this context. Such a fact is important since it emphasizes the ability to use the hematite as additional bridging material. Further, the rheological analysis demonstrated that variations in PSD elicited only slight changes in the drilling fluid's rheological parameters, suggesting robustness in its behavior against PSD alterations. Notably, the Herschel−Bulkley model emerged as the most accurate in capturing the fluid's shear-thinning behavior, highlighting its suitability for modeling such complex fluids. A key insight from this research was the identification of the particle size ratio (D_{90}/D_{10}) as a crucial factor in governing the filtration properties and the characteristics of the filter cake. This ratio exhibited a significant correlation with these properties, offering a promising avenue for targeted manipulation of PSD to optimize drilling fluid performance. The study's findings not only shed light on the intricate interplay between hematite PSD and drilling fluid properties but also opened avenues for refining filtration processes and enhancing the efficiency and effectiveness of drilling operations. Future work will investigate additional factors, including mud density variation, test conditions, and weighting material type.

AUTHOR INFORMATION

Corresponding Author

Badr Bageri − *Center for Integrative Petroleum Research, King Fahd University of Petroleum and Minerals, Dhahran 31261, Saudi Arabia; Department of Petroleum Engineering, King Fahd University of Petroleum and Minerals, Dhahran 31261, Saudi Arabia;* orcid.org/0000-0002-7510-0933; Phone: +966 535101971; Email: badr.bageri@kfupm.edu.sa; Fax: +966 13 860 3888

Authors

Jaber Al Jaberi − *Center for Integrative Petroleum Research, King Fahd University of Petroleum and Minerals, Dhahran 31261, Saudi Arabia*

Waleed Otain − *Department of Petroleum Engineering, King Fahd University of Petroleum and Minerals, Dhahran 31261, Saudi Arabia*

Anas Alsaleem − *Department of Petroleum Engineering, King Fahd University of Petroleum and Minerals, Dhahran 31261, Saudi Arabia*

Abdulrauf Rasheed Adebayo − *Center for Integrative Petroleum Research, King Fahd University of Petroleum and Minerals, Dhahran 31261, Saudi Arabia*

Complete contact information is available at: https://pubs.acs.org/10.1021/acsomega.4c02352

Notes

The authors declare no competing financial interest.

ACKNOWLEDGMENTS

We acknowledge the research support of College of Petroleum Engineering Geosciences at King Fahd University of Petroleum Minerals.

REFERENCES

(1) Gutzmer, J.; Beukes, N. J. Earliest laterites and possible evidence for terrestrial vegetation in the Early Proterozoic. *Geology* **1998**, *26*, 263−266.

(2) Beukes, N. J.; Gutzmer, J.; Mukhopadhyay, J. The geology and genesis of high-grade hematite iron ore deposits, Transactions of the Institution of Mining and Metallurgy, Section B. *Applied Earth Science* **2003**, *112*, 18−25.

(3) Beukes, N.J.; Dorland, H.; Gutzmer, J.; Nedachi, M. *Tropical laterites, life on land, and the history of atmospheric oxygen in the Paleoproterozoic*, 2002. http://pubs.geoscienceworld.org/gsa/geology/article-pdf/30/6/491/3523039/i0091-7613-30-6-491.pdf.

(4) Zhu, C.; Li, C.; Zheng, M.; Delaunay, J. J. Plasma-Induced Oxygen Vacancies in Ultrathin Hematite Nanoflakes Promoting Photoelectrochemical Water Oxidation. *ACS Appl. Mater. Interfaces* **2015**, *7*, 22355−22363.

(5) Linderholm, C.; Schmitz, M.; Knutsson, P.; Källén, M.; Lyngfelt, A. Use of low-volatile solid fuels in a 100 kW chemical-looping combustor. *Energy Fuels* **2014**, *28*, 5942−5952.

(6) Rajendran, R.; Yaakob, Z.; Pudukudy, M.; Rahaman, M. S. A.; Sopian, K. Photoelectrochemical water splitting performance of vertically aligned hematite nanoflakes deposited on FTO by a hydrothermal method. *J. Alloys Compd.* **2014**, *608*, 207−212.

(7) Iandolo, B.; Wickman, B.; Zorić, I.; Hellman, A. The rise of hematite: origin and strategies to reduce the high onset potential for the oxygen evolution reaction. *J. Mater. Chem. A Mater.* **2015**, *3*, 16896−16912.

(8) Ahmad, W. R. W.; Mamat, M.H.; Zoolfakar, A.S.; Khusaimi, Z.; Rusop, M.; Alam, S. A Review on Hematite α-Fe 2 O 3 Focusing on Nanostructures, Synthesis Methods and Applications. In *2016 IEEE Student Conference on Research and Development (SCOReD)*; IEEE, **2016**.

(9) Wu, Y.; Xia, C.; Zhang, W.; Yang, X.; Bao, Z. Y.; Li, J. J.; Zhu, B. Natural Hematite for Next-Generation Solid Oxide Fuel Cells. *Adv. Funct Mater.* **2016**, *26*, 938−942.

(10) Eggleston, C. M. Toward New Uses for Hematite. *Science* **1979**, *320* (2008), 183−184.

(11) Ahmed, N.; Alam, M. S.; Salam, M. A. Experimental analysis of drilling fluid prepared by mixing iron (III) oxide nanoparticles with a

KCl−Glycol−PHPA polymer-based mud used in drilling operation. *J. Pet Explor Prod Technol.* **2020**, *10*, 3389−3397.
(12) Scharf, A.D.; Watts, A.D. *SPE ltabirite: An Alternative Weighting Material for Heavy Oil-Base Muds*, 1984. http://onepetro.org/SPEATCE/proceedings-pdf/84SPE/All-84SPE/SPE-13159-MS/3261352/spe-13159-ms.pdf/1.
(13) Tovar, J.; Rodríguez, Z.; Quiroga, F.; Greaves, R.; Meléndez, H.; Arocha, J.; Bland, R.; Hebert, M. ORIMATITAO®. An improved hematite for drilling fluids. In *SPE Latin American and Caribbean Petroleum Engineering Conference Proceedings 1999-Jan*, 1999.
(14) Fadl, A. M.; Abdou, M. I.; El-Sayed Ahmed, H.; Wahab Gaber, M. A. Delaminated iron ore (hematite-Barite) as alternative weighting agent to Barite in petroleum drilling fluids engineering operations and mechanism study. *Ain Shams Engineering Journal* **2020**, *11*, 1317−1337.
(15) Quercia, G.; Belisario, R.; Rengifo, R. Reduction of erosion rate by particle size distribution (PSD) modification of hematite as weighting agent for oil based drilling fluids. *Wear* **2009**, *266*, 1229−1236.
(16) Tehrani, A.; Cliffe, A.; Hodder, M.H.; Young, S.; Lee, J.; Stark, J.; Seale, S. Alternative drilling fluid weighting agents: A comprehensive study on ilmenite and hematite. In *SPE/IADC Drilling Conference, Proceedings*; SPE, 2014; pp. 222−239.
(17) Kang, Y.; Tan, Q.; You, L.; Zhang, X.; Xu, C.; Lin, C. Experimental investigation on size degradation of bridging material in drilling fluids. *Powder Technol.* **2019**, *342*, 54−66.
(18) Haider, G.; Othayq, M.; Zhang, J.; Vieira, R.E.; Shirazi, S.A. Effect of particle size on erosion measurements and predictions in annular flow for an elbow. *Wear* **2021**, *476*, No. 203579.
(19) Bageri, B. S.; Gamal, H.; Elkatatny, S.; Patil, S. Effect of Different Weighting Agents on Drilling Fluids and Filter Cake Properties in Sandstone Formations. *ACS Omega* **2021**, *6*, 16176−16186.
(20) Adebayo, A. R.; Bageri, B. S. A simple NMR methodology for evaluating filter cake properties and drilling fluid-induced formation damage. *J. Pet Explor Prod Technol.* **2020**, *10*, 1643−1655.
(21) Adebayo, A. R.; Bageri, B. S.; Al Jaberi, J.; Salin, R. B. A calibration method for estimating mudcake thickness and porosity using NMR data. *J. Pet Sci. Eng.* **2020**, *195*, No. 107582.
(22) Bageri, B. S.; Adebayo, A. R.; Al Jaberi, J.; Patil, S. Effect of perlite particles on the filtration properties of high-density Barite weighted water-based drilling fluid. *Powder Technol.* **2020**, *360*, 1157−1166.
(23) Kolodzie, S. Analysis of Pore Throat Size and Use of the Waxman-Smits Equation To Determine Ooip in Spindle Field, Colorado. In *Paper presented at the SPE Annual Technical Conference and Exhibition, Dallas, Texas*; Society of Petroleum Engineers of AIME, 1980.
(24) Klungtvedt, K. R.; Saasen, A. The Role of Particle Size Distribution for Fluid Loss Materials on Formation of Filter-Cakes and Avoiding Formation Damage. *Journal of Energy Resources Technology, Transactions of the ASME* **2023**, *145*, 1−10.
(25) Kleinberg, R. L. Utility of NMR T2 distributions, connection with capillary pressure, clay effect, and determination of the surface relaxivity parameter $\rho 2$. *Magn Reson Imaging* **1996**, *14*, 761−767.
(26) Keating, K.; Knight, R. A laboratory study of the effect of magnetite on NMR relaxation rates. *J. Appl. Geophy* **2008**, *66*, 188−196.
(27) Robertson, R. E.; Stiff, H. A. An Improved Mathematical Model for Relating Shear Stress to Shear Rate in Drilling Fluids and Cement Slurries. *Society of Petroleum Engineers Journal* **1976**, *16*, 31−36.
(28) Skelland, A. H. P. Non-Newtonian flow and heat transfer (Book on quantitative relationships for non- Newtonian systems, considering classification and fluid behavior of materials with anomalous flow properties). *Int. J. Heat Mass Transf.* **1968**, *11*, 1213.
(29) Eugene, C. *Bingham, Fluidity and plasticity*, 1st ed.; McGraw-Hill Book Company, Inc.: New York, 1922.
(30) Mitchell, R.; Miska, S. *Fundamentals of drilling engineering*; SPE, 2011.

https://doi.org/10.1021/acsomega.4c02352
ACS Omega 2024, 9, 25084−25093